NeuroImage 59 (2012) 3582–3593

Contents lists available at SciVerse ScienceDirect

NeuroImage

journal homepage: www.elsevier.com/locate/ynimg

Quantitative PET analyses of regional [^{11}C]PE2I binding to the dopamine transporter — Application to juvenile myoclonic epilepsy

Ikuo Odano [a,c,*], Andrea Varrone [a], Ivanka Savic [b], Carolina Ciumas [b], Per Karlsson [a], Aurelija Jucaite [a], Christer Halldin [a], Lars Farde [a]

[a] Psychiatric Section, Department of Clinical Neuroscience Karolinska Institutet, Stockholm, Sweden
[b] Department of Neurobiology, Karolinska University Hospital, Stockholm, Sweden
[c] Division of Functional Imaging, Department of Sensory and Integrative Medicine. Niigata University Graduate School of Medicine and Dental Sciences, Niigata, Japan

ARTICLE INFO

Article history:
Received 3 June 2011
Revised 17 October 2011
Accepted 20 October 2011
Available online 28 October 2011

Keywords:
Dopamine transporter
^{11}C-PE2I
Juvenile myoclonic epilepsy
Epilepsy
Modeling
Reference tissue model
Neuroreceptor imaging
PET

ABSTRACT

The dopamine transporter (DAT) is of central interest in research on the pathophysiology and treatment of neuro-psychiatric disorders. [^{11}C]PE2I is an established radioligand that provides high-contrast delineation of brain regions that are rich in DAT. The aim of the present PET study in eight patients with juvenile myoclonic epilepsy (JME) was to evaluate the kinetics of [^{11}C]PE2I in the brain and to compare binding parameters with those of age-matched control subjects (n = 6). Each patient participated in 90-minute PET measurements with [^{11}C]PE2I. Data were analyzed using kinetic compartment analyses with metabolite-corrected arterial plasma input and reference tissue models using the cerebellum as a reference region. The time-activity curves were well described by the two-tissue compartment model (2TCM) for the DAT-rich regions. The 2TCM with fixed K_1/k_2 ratio derived from the cerebellum provided robust and reliable estimates of binding potential (BP_{ND}) and total distribution volume (V_T). The reference tissue models also provided robust estimates of BP_{ND}, although they gave lower BP_{ND} values than the kinetic analysis. Compared with those of control subjects, we found that BP_{ND} values obtained by all approaches were reduced in the midbrain of the patients with JME. The finding indicates impaired dopamine uptake in the midbrain of JME patients. The three-tissue compartment model could best describe uptake in the cerebellum, indicating that two kinetically distinguishable compartments exist in cerebellar tissue, which may correspond to nonspecific binding and the blood–brain barrier passing metabolite. The reference tissue models should be applied with better understanding of the biochemical nature of the radioligand and the reliability of these approaches.

Introduction

The dopamine transporter (DAT) plays an important role in the reuptake of dopamine into pre-synaptic nerves and regulates dopaminergic transmission in the synaptic cleft. Molecular imaging with positron emission tomography (PET) is a well established tool to evaluate dopaminergic function (Allard et al., 1990; Antonini et al., 2001; Ginovart et al., 1997; Laakso et al., 2001; Meyer et al., 2001; Volkow et al., 2002; Wong et al., 1998).

Among several radioligands for in vivo DAT imaging developed for PET (Chalon et al., 2006; Farde et al., 1994; Goodman et al., 2000; Halldin et al., 1996; Müller et al., 1993; Varrone and Halldin, 2010; Varrone et al., 2009; Wong et al., 1993), [^{11}C]PE2I is an established radioligand with high affinity and selectivity for DAT (Emond et al., 1997; Guilloteau et al., 2003) and has been applied for not only normal human brain but also neuro-psychiatric disorders with quantitative approaches (Arakawa et al., 2009; Ciumas et al., 2008; Ciumas et al., 2010; Halldin et al., 2003; Hirvonen et al., 2008; Jucaite et al., 2005; Jucaite et al., 2006; Leroy et al., 2007; Seki et al., 2010).

More recently, [^{11}C]PE2I and PET studies were performed on patients with juvenile myoclonic epilepsy (JME), and binding potential (BP_{ND}), a parameter for specific binding at equilibrium, was measured (Ciumas et al., 2008). As a result, regional BP_{ND} was found to be reduced in the midbrain and substantia nigra, but not in the striatum, compared with that of age-matched control subjects. These findings suggest that that dopamine signaling is impaired in patients with JME, and a follow up study with an extended number of JME patients (Ciumas et al., 2010) showed that this impairment was related to the breakdown in cognitive control in JME patients. The measuring method applied in these studies was the simplified reference tissue model (SRTM) (Lammertsma and Hume, 1996), a non-invasive approach without arterial plasma input, in which the cerebellum was used as a reference region.

Two potential limitations are, however, suggested for quantification with [^{11}C]PE2I and PET, one of which is late peak equilibrium,

* Corresponding author at: Division of Functional Imaging, Department of Sensory and Integrative Medicine, Niigata University Graduate School of Medicine and Dental Sciences, Asahimachi-dori Niigata, 951-8510, Japan.
E-mail address: ikuomi@aurora.ocn.ne.jp (I. Odano).

1053-8119/$ – see front matter © 2011 Elsevier Inc. All rights reserved.
doi:10.1016/j.neuroimage.2011.10.067

and the other is radiolabeled metabolite that passes the blood–brain barrier and potentially binds to the DAT, as reported in a rodent experiment (Shetty et al., 2007), but not yet in human brain. These limitations probably make it difficult to obtain robust and reliable values of binding parameters.

The purpose of the present extended analysis was to examine [^{11}C]PE2I uptake in the patients with JME, to measure binding parameters by applying the established kinetic compartment analysis using metabolite-corrected arterial plasma input, to compare the kinetics and binding parameters with those of control subjects, to confirm binding potential reduction in JME patients previously detected, and to evaluate the reliability of non-invasive reference tissue models using the cerebellum as a reference. Particular emphasis was placed on evaluating the binding parameters in the midbrain, the kinetics of [^{11}C]PE2I in the cerebellum as a reference region and additional information about the pathophysiology of JME.

Materials and methods

Patients

The study was approved by the ethics committee of Karolinska Hospital. Eight patients with JME participated in the study, six men and two women, aged 20–56 years (mean ± s.d., 39 ± 12). JME was diagnosed according to the International Classification of Epilepsies from 1989, on the basis of seizure history, seizure semiology as described by relatives or recorded during hospitalization, and results of scalp EEG, the details of which were described previously (Ciumas et al., 2008). The clinical characteristics of the patients and medication are listed in Table 1. Seven patients were medicated with Valproate, but one (patient E) had no medication.

Control subjects

Six men, aged 19–38 years (mean ± s.d., 34 ± 11), were used as control subjects investigated in a previous study (Jucaite et al., 2006).

Radiochemistry

The acid precursor of PE2I was prepared and radiolabeled by O-methylation using [^{11}C]methyl triflate as described in detail elsewhere (Halldin et al., 2003). The decay-corrected radiochemical yield of [^{11}C]PE2I was 50%. The radiochemical purity of the final product was >99%. The specific radioactivity of [^{11}C]PE2I at the time of injection was between 125 and 374 GBq/μmol (mean ± s.d., 220 ± 106 GBq/μmol). The radioactivity injected ranged from 307 to 396 MBq (mean ± s.d., 364 ± 29 MBq) and the injected mass was between 0.42 μg and 1.3 μg (mean ± s.d., 0.86 ± 0.37 μg). The radioligand was injected as a rapid bolus.

MRI and regions of interest

T1-weighted MR images were acquired using a 1.5 T Signa unit (General Electric, Milwaukee). A standard spin-echo sequence with a 256 × 256 matrix and 1 mm slice thickness was used with a repetition time of 400 ms. Echo times were 9 ms for images. A head fixation system was used for both MRI and PET measurements (Bergstrom et al., 1981). Regions of interest (ROIs) were outlined manually on each individual MR image and transferred to the corresponding PET images showing the distribution of [^{11}C]PE2I (Roland et al., 1994). Each ROI set consisted of both sides of caudate and putamen, the midbrain and the cerebellum, as shown in Fig. 1.

Table 1
The list of patients with JME and medication.

Patients	Sex	Age	Medication
A	m	56	Valproate
B	m	45	Valproate
C	m	30	Valproate, Lamotrigine
D	m	42	Valproate, Lamotrigine
E	f	32	No medication
F	f	49	Valproate, Lamotrigine
G	m	20	Valproate, Leviteracetam
H	m	40	Valproate

PET experimental procedure

The PET system (Siemens ECAT Exact HR 47, Siemens/CTI, TN) has been described previously (Jucaite et al., 2006). All PET measurements were carried out in the interictal state for the patients with JME, which was evaluated by the neurologists present during each experiment.

The last seizure (including myoclonia) was reported to be at least 1 week before the PET scan.

Brain radioactivity of the patient with JME was measured in a series of consecutive time frames for 90 min. The frame sequence consisted of eight fifteen-second frames, eight one-minute frames, four two-minute frames, four four-minute frames, four six-minute frames and four eight-minute frames. On the other hand, radioactivity in the brain of a normal subject was measured for 63 min, with three one-minute frames, four three-minute frames and eight six-minute frames.

Arterial blood sampling

To obtain the arterial input function, an automated blood sampling system (ABSS; Scanditronix, Uppsala, Sweden) was used during the first 5 min of each PET measurement. After the first 5 min, arterial blood samples (2 ml) were taken manually at the midpoint of each frame until the end of the measurement (Farde et al., 1989).

Plasma metabolite analysis (HPLC) of [^{11}C]PE2I

The fractions of plasma activity corresponding to unchanged [^{11}C]PE2I and labeled metabolites were determined as described previously (Halldin et al., 2003). Arterial blood samples (2 ml) were drawn at set times: 4, 10, 20, 30, 40, 50 and 60 min after i.v. injection of [^{11}C]PE2I. The in vivo assay of radioactive metabolites was performed using standard procedures developed at Karolinska Institutet for new PET radioligands (Halldin et al., 1995). In short, the supernatant liquid obtained after centrifugation for 2 min was deproteinized with acetonitrile. It was then analyzed by gradient high performance liquid chromatography (HPLC) on a reverse-phase column (Waters μ-Bondapak C18, 7.8 × 300 mm, 10 μm) and eluted at 6 ml/min over 8 min with acetonitrile/0.01 mol/l phosphoric acid, using a gradient of 25/75 to 80/20 from 0 to 4.5 min and 80/20 to 30/70 from 4.5 to 8 min.

The individual time-activity curves (TACs) for fraction (%) of radioactivity in plasma that corresponds to unchanged [^{11}C]PE2I were obtained by fitting with the Hill's function described as follows:

$$m(t) = \left(1 - \frac{\beta t^{\delta}}{t^{\delta} + \gamma}\right) \times 100, \quad (1)$$

where m(t) is percentage of the metabolite fraction in the plasma and β, γ and δ are the parameters of the function form to be estimated under the conditions of $0 < \beta \leq 1$, $0 < \delta$ and $0 < \gamma$ (Gunn et al., 1998; Hill, 1910). Finally, each metabolite-corrected arterial plasma input was derived by multiplying uncorrected plasma input by the function m(t).

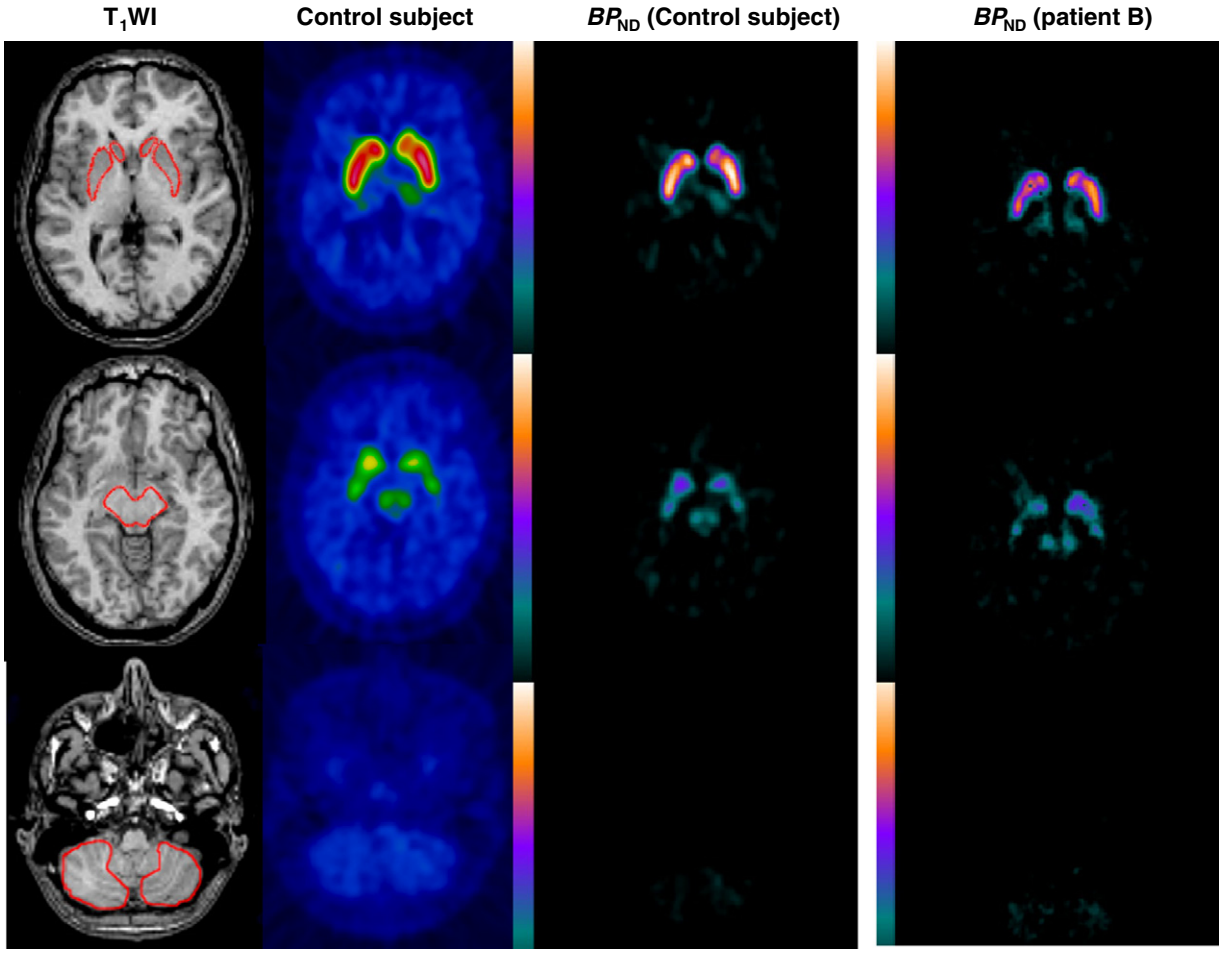

Fig. 1. The summation images of [^{11}C]PE2I after i.v., injection, MR images and BP_{ND} images of a representative control subject, and BP_{ND} images of 45-year-old man with JME (patient B). The regions of interest were manually drawn on the putamen, the caudate, the midbrain and the cerebellum. No normalization was performed. BP_{ND} images were obtained by the automated receptor imaging system (ARIS).

Invasive and non-invasive approaches

To examine [^{11}C]PE2I binding in brain, we employed established quantitative approaches. Kinetic compartment analysis is an approach dependent on a metabolite-corrected arterial plasma curve as the input function. The simplified reference tissue model (SRTM) and non-invasive linear graphical analysis (Logan DVR) using the cerebellum as a reference region are referred to as reference tissue approaches.

Kinetic analysis with the two-tissue and three-tissue compartment models (2TCM and 3TCM)

The kinetic behavior of [^{11}C]PE2I was analyzed using the conventional three-tissue compartment model (3TCM) as shown in Fig. 2 (Farde et al., 1998). The three-tissue compartments correspond to the radioactivity concentrations of unchanged radioligand in plasma (C_P), free (unbound) radioligand in brain (C_F), nonspecifically bound radioligand (C_{NS}) and radioligand specifically bound to receptors (C_S). The rate constants K_1 and k_2 correspond to the influx and outflux rates of the radioligand across the blood–brain barrier, respectively. The rate constants k_3 and k_4 correspond to the rates for radioligand transfer between the compartments for free and specific radioligand binding to receptors, respectively. The rate constants for k_5 and k_6 correspond to the rates for radioligand transfer between the compartments for free and nonspecifically bound radioligand, respectively. All concentrations are expressed in units of nCi/ml. K_1 has units of ml/min/ml of brain tissue and k_2 through k_6 have units of min^{-1}. The blood volume component has been estimated as 0.04 (Farde et al., 1989). To decrease variations of parameters, a common assumption was applied, in which the two compartments C_F and C_{NS} rapidly reach a steady state to form one effective compartment (Logan et al., 1987; Wong et al., 1986). The resulting compartment (C_{ND}) corresponds to nondisplaceable radioligands in brain. The simplified model with two tissue compartments and four first-order rate constants, K_1, k_2, k_3 and k_4, the 2TCM, was used to describe the regional time-activity curves (TACs) for [^{11}C]PE2I binding.

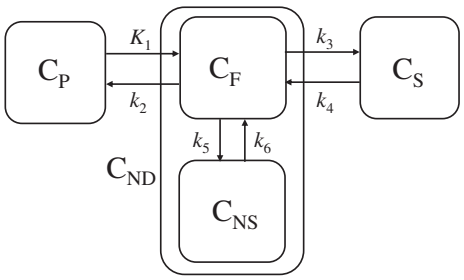

Fig. 2. The three-tissue compartment model (3TCM) used to describe the kinetics of [^{11}C]PE2I in the brain.

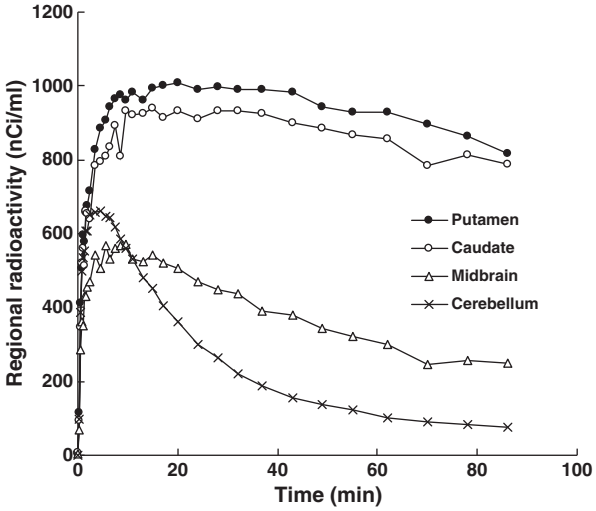

Fig. 3. Time-activity curves for regional brain radioactivity after intravenous injection of 396 MBq of [^{11}C]PE2I in 45-year-old man with JME (patient B).

The four rate constants of the 2TCM and six of the 3TCM were determined by weighted nonlinear least squares fitting technique with constraints restricting parameters between 0 and 1.0 using the PMOD software (PMOD Technologies Ltd., Zurich, Switzerland). We also applied the 2TCM and 3TCM to fit the TACs for the cerebellum.

Binding potential

After injection of a radioligand with high specific radioactivity, the receptor density (B_{max}) to affinity (K_D) ratio corresponds to the ratio of k_3 to k_4 in the 2TCM and the 3TCM, and is referred to as the binding potential (Mintun et al., 1984). The binding potential (BP_{ND}) is defined as follows:

$$BP_{ND} = f_{ND} \cdot \frac{B_{max}}{K_D} = \frac{k_3}{k_4}, \tag{2}$$

where f_{ND} is the free fraction of radioligand in the nondisplaceable compartment (Innis et al., 2007), the term of which is equal to f_2. Since the fraction of radioligand that is unbound to plasma proteins was not measured in the present studies, the value of f_{ND} was not included in the analysis.

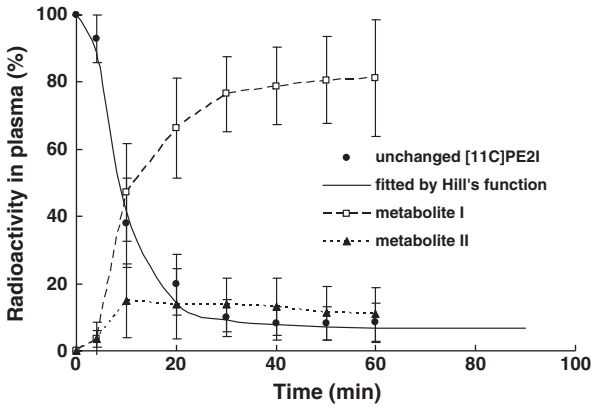

Fig. 4. Time-activity curves (TACs) for fraction (%) of radioactivity in plasma that represent unchanged [^{11}C]PE2I, mean TAC fitted by Hill's function and two metabolites (mean ± s.d., n = 8). Individual fitted curve for unchanged [^{11}C]PE2I was used to establish metabolite-corrected arterial plasma input.

Distribution volume

[^{11}C]PE2I binding was also described using the concept of total distribution volume, V_T, which is defined by the following equation for the 2TCM:

$$V_T = \frac{K_1}{k_2}\left(1 + \frac{k_3}{k_4}\right), \tag{3}$$

and for the 3TCM:

$$V_T = \frac{K_1}{k_2}\left(1 + \frac{k_3}{k_4} + \frac{k_5}{k_6}\right). \tag{4}$$

Kinetic analysis with the one-tissue compartment model (1TCM)

If binding and dissociation at the specific binding compartment (C_S) are rapid compared to the transport parameters K_1 and k_2, the model can be reduced to two compartments. Thus, the single tissue compartment contains free, nonspecifically bound, and specifically bound ligand. In this manner, there will be only two rate constants, K_1 and k_2'. The rate constant k_2' corresponds to the efflux rate, and

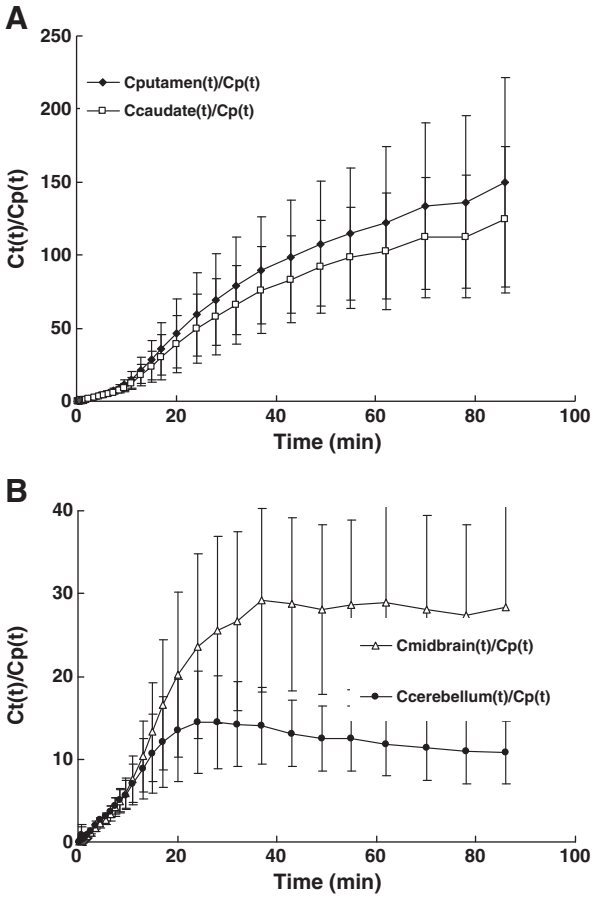

Fig. 5. Tissue-to-plasma concentration ratios, $C_t(t)/C_p(t)$, for the putamen, caudate, midbrain and the cerebellum (mean ± s.d., n = 8). Note that ratios reached an almost steady state at 40–60 min for the midbrain and at 20–30 min for the cerebellum (B).

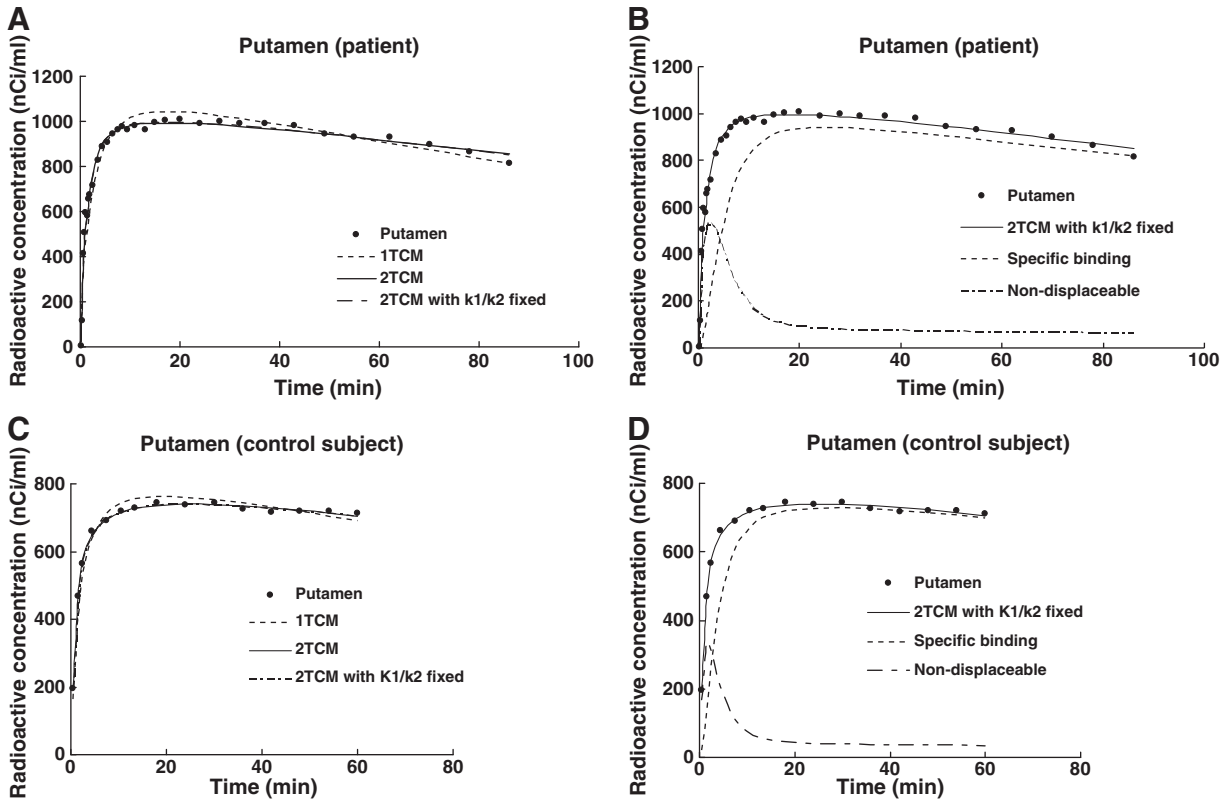

Fig. 6. (A) and (C) Radioactivity vs. time in the putamen of patient B and the representative control subject after i.v. injection of [^{11}C]PE2, and curve fits of the 1TCM, the 2TCM, the 2TCM with a fixed K_1/k_2 ratio obtained from cerebellum. (B) and (D) Total binding, specific binding (C_S), non-displaceable concentration (C_{ND}) in the putamen of the patient B and the control subject as estimated by the 2TCM with a fixed K_1/k_2 ratio obtained from cerebellum.

its relation to k_2, k_3 and k_4 of the 2TCM is given by the following equation:

$$k_2' = \frac{k_2}{1 + k_3/k_4}. \quad (5)$$

The two-tissue compartment model with fixed K_1/k_2 for cerebellum, 2TCM(2)

In this configuration, the partition coefficient, K_1/k_2, was assumed to be equal in all brain regions. The K_1/k_2 ratio was obtained from the one-tissue compartment model analysis of the cerebellum, and was then entered into the two-tissue compartment model analysis of each ROI (Lundberg et al., 2005; Odano et al., 2009a). The rate constants, binding potential and total distribution volume values were obtained according to the definition described above.

Simplified reference tissue model (SRTM)

According to the SRTM (Gunn et al., 1998; Lammertsma and Hume, 1996), the binding potential, BP_{ND}, is obtained using the following equation:

$$C_t(t) = R_1 \cdot C_{ref}(t) + k_2\left(1 - \frac{R_1}{1 + BP_{ND}}\right) \cdot C_{ref}(t) \otimes \exp\left(-\frac{k_2 \cdot t}{1 + BP_{ND}}\right), \quad (6)$$

where R_1 is the ratio of K_1/K'_1 (K_1: influx rate constant for the target tissue, K'_1: influx rate constant for the reference tissue), and $C_t(t)$ and $C_{ref}(t)$ are TACs for the target and reference tissues, respectively. In this approach, the cerebellum was used as the reference tissue. The symbol ⊗ denotes the convolution integral.

Non-invasive linear graphical approach (Logan DVR)

In the non-invasive linear graphical analysis, the cerebellum was also used as a reference region. Radioactivity in this tissue region was integrated over time and normalized to the last frame for the tissue radioactivity. The integrated value was plotted vs. integrated and normalized radioactivity for the cerebellum. For a reversible radioligand, this plot becomes linear and the asymptote of the slope equals to the distribution volume ratio DVR (Logan et al., 1996). The binding potential, BP_{ND}, was estimated as follows:

$$BP_{ND} = DVR - 1. \quad (7)$$

Statistics

Compartment model levels of complexity were compared using three statistical methods; the Akaike information criterion (Akaike, 1974), the Schwarz criterion (Schwarz, 1978) and F statistics (Carson, 1986; Farde et al., 1989; Landaw and DiStefano, 1984). Statistical significance using the F-test was assumed for p values less than or equal to 0.05. The standard error of the parameter was given by the diagonal of the covariance matrix (Carson, 1986), expressed as a percentage of the parameter value (coefficient of variation, %COV), and used to validate the parameter by a non-linear least squares fitting procedure (Ginovart et al., 2006). Differences of binding parameters between patients and control subjects were tested with unpaired t test when

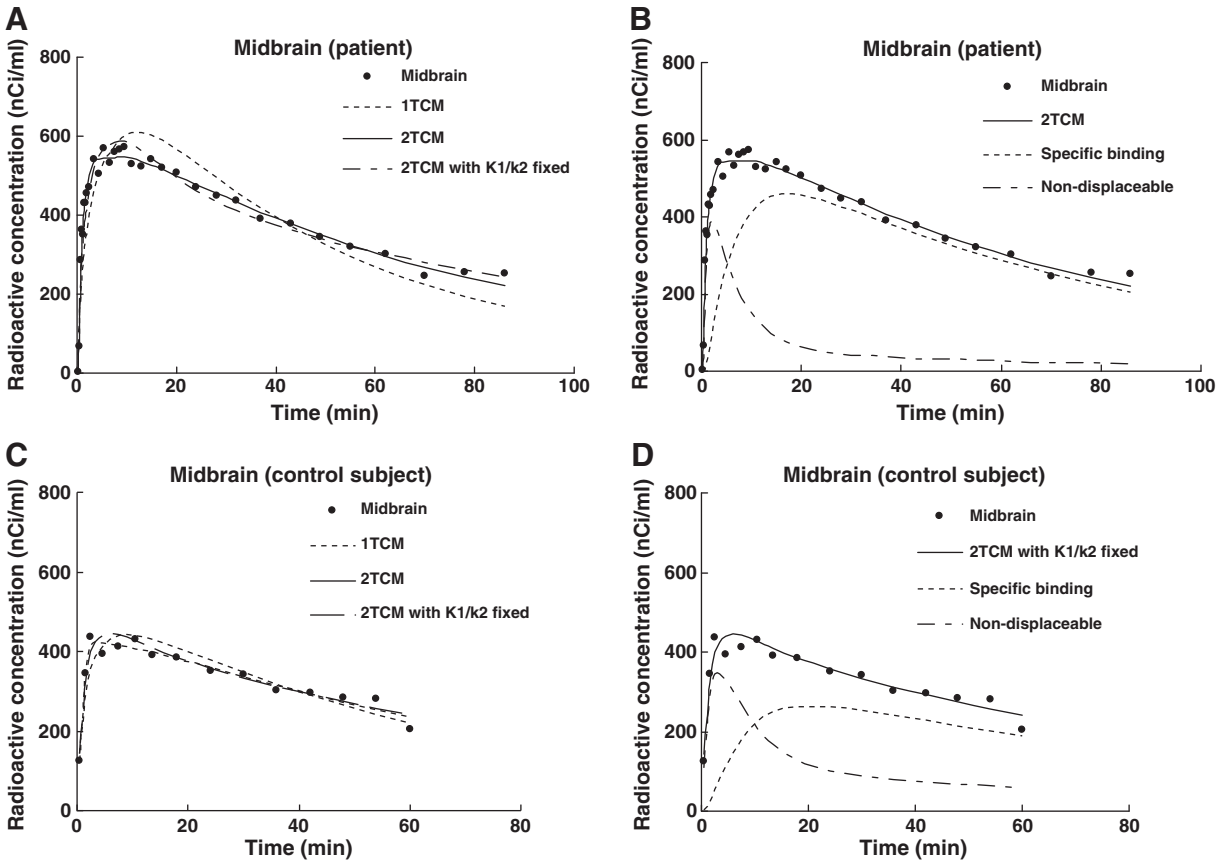

Fig. 7. (A) and (C) Radioactivity vs. time in the midbrain of patient (B) and the representative control subject after i.v. injection of [^{11}C]PE2I, and curve fits of the 1TCM, the 2TCM, the 2TCM with a fixed K_1/k_2 ratio obtained from cerebellum. (B) and (D) Total binding, specific binding (C_S), non-displaceable concentration (C_{ND}) in the midbrain of the patient B and the control subject as estimated by the 2TCM with a fixed K_1/k_2 ratio obtained from cerebellum.

samples had possibly equal variances, and otherwise Welch's *t* test was used. Significance was determined at $p<0.05$.

Data analysis and comparison

Since the data of the control subjects were acquired for 63 min after the radioligand injection, the data of patients with JME were analyzed not only for 90 min, but also for 58 min, and binding parameters obtained were compared.

Results

After intravenous injection of [^{11}C]PE2I, the radioactivity appeared rapidly and high radioactivity was observed in the putamen and the

Table 2
Binding parameters obtained by kinetic analysis of [^{11}C]PE2I binding in 90 min data acquisition for the patients with JME. Note that %COVs of k_3/k_4 for the 2TCM(2) were lower than those for the 2TCM, and were<10%, showing high robustness.

		K_1	k_2	k_3	k_4	k_5	k_6	k_3/k_4	k_5/k_6	V_T
Mean ± s.d. (n = 8)										
Putamen	2TCM	0.41 ± 0.09	0.10 ± 0.03	0.33 ± 0.18	0.02 ± 0.01			14 ± 4.8		62 ± 23
	2TCM(2)	0.41 ± 0.09	0.12 ± 0.03	0.37 ± 0.17	0.02 ± 0.01			16 ± 4.4		60 ± 23
Caudate	2TCM	0.36 ± 0.10	0.12 ± 0.04	0.35 ± 0.14	0.02 ± 0.01			16 ± 4.9		52 ± 18
	2TCM(2)	0.36 ± 0.10	0.11 ± 0.03	0.32 ± 0.13	0.02 ± 0.01			14 ± 3.5		53 ± 18
Midbrain	2TCM	0.26 ± 0.07	0.12 ± 0.03	0.12 ± 0.05	0.05 ± 0.01			2.6 ± 0.8		8.1 ± 1.9
	2TCM(2)	0.24 ± 0.06	0.07 ± 0.01	0.06 ± 0.02	0.04 ± 0.01			1.4 ± 0.2		8.4 ± 1.9
Cerebellum	2TCM	0.35 ± 0.07	0.17 ± 0.04	0.06 ± 0.05	0.06 ± 0.02			1.0 ± 0.4		4.2 ± 0.9
	3TCM	0.42 ± 0.09	0.51 ± 0.29	0.07 ± 0.03	0.03 ± 0.01	0.59 ± 0.27	0.36 ± 0.13	2.1 ± 0.9	1.9 ± 1.1	4.4 ± 0.8
%COV Putamen	2TCM	3.1 ± 2.1	20 ± 12	14 ± 5.8	16 ± 6.8			19 ± 12		5.3 ± 2.6
	2TCM(2)	2.5 ± 1.6		6.9 ± 2.9	11 ± 4.0			5.0 ± 2.0		4.8 ± 1.9
Caudate	2TCM	4.3 ± 1.5	23 ± 9.3	22 ± 6.9	25 ± 11			23 ± 8.8		7.9 ± 2.6
	2TCM(2)	3.1 ± 1.2		15 ± 8.3	21 ± 8.0			8.4 ± 2.8		7.9 ± 2.6
Midbrain	2TCM	3.2 ± 1.4	15 ± 14	25 ± 23	16 ± 10			18 ± 16		4.5 ± 2.8
	2TCM(2)	4.8 ± 6.4		15 ± 6.8	21 ± 8.5			9 ± 3.2		5.7 ± 1.9
Cerebellum	2TCM	2.0 ± 1.1	6.8 ± 5.3	18 ± 7.2	13 ± 3.9			10 ± 5.8		2.6 ± 1.1
	3TCM	2.8 ± 1.9	14 ± 9.7	35 ± 32	25 ± 20	18 ± 14	20 ± 9.1	–	–	–

2TCM: the two-tissue compartment model.
2CM(2): the two-tissue compartment model with K_1/k_2 fixed for cerebellum.
3TCM: the three-tissue compartment model.
V_T: total distribution volume.
%COVs of k_3/k_4, k_5/k_6 and total V_T for 3TCM were not obtained by this software.

Table 3
Comparison of binding potential, k_3/k_4 and BP_{ND}, calculated for 90 min and for 58 min of the data of the patients with JME (n = 8).

	Data analysis		Acquisition 0–90 min	(%COV)	Acquisition 0–58 min	(%COV)	Statistics
Putamen	2TCM	k_3/k_4	14 ± 4.8	19 ± 12	16 ± 6.6	24 ± 11	ns
	2TCM(2)	k_3/k_4	16 ± 4.4	5.0 ± 2.0	18 ± 6.7	11 ± 4.2	ns
	SRTM	BP_{ND}	7.5 ± 1.3	2.9 ± 1.1	6.8 ± 1.1	5.4 ± 2.5	p<0.001
	Logan DVR	BP_{ND}	8.1 ± 1.5	–	7.5 ± 1.2	–	p<0.005
Caudate	2TCM	k_3/k_4	16 ± 4.9	23 ± 8.8	19 ± 6.7	51 ± 31	ns
	2TCM(2)	k_3/k_4	14 ± 3.5	8.4 ± 2.8	18 ± 7.5	23 ± 9.4	ns
	SRTM	BP_{ND}	6.2 ± 1.0	4.7 ± 1.4	6.1 ± 1.1	10 ± 2.7	ns
	Logan DVR	BP_{ND}	6.7 ± 1.1	–	6.9 ± 1.3	–	ns
Midbrain	2TCM	k_3/k_4	2.6 ± 0.8	18 ± 16	2.8 ± 0.5	23 ± 13	ns
	2TCM(2)	k_3/k_4	1.4 ± 0.2	9.0 ± 3.2	1.5 ± 0.3	20 ± 11	ns
	SRTM	BP_{ND}	0.8 ± 0.1	5.6 ± 1.6	0.7 ± 0.1	9.1 ± 3.7	ns
	Logan DVR	BP_{ND}	0.8 ± 0.1	–	0.8 ± 0.1	–	ns

2TCM: the two-tissue compartment model.
2TCM(2): the two-tissue compartment model with K_1/k_2 fixed for cerebellum.
Values are mean ± s.d.
ns: not significant.
SRTM: simplified reference tissue model.
Logan DVR: non-invasive linear graphic approach.
%COVs for Logan DVR were not obtained by this software.

Table 4
Comparison of binding potential, k_3/k_4, for [^{11}C]PE2I binding calculated by the two-tissue compartment model and the two-tissue compartment model with K_1/k_2 fixed for cerebellum of the control subjects and patients with JME.

		Control subjects (n = 6)		Patients with JME (n = 8)		Statistics	Mean reduction (%)
Acquisition time		0–63 min		0–58 min			
Kinetic analysis		k_3/k_4	(%COV)	k_3/k_4	(%COV)		
Putamen	2TCM	19 ± 4.5	28 ± 14	16 ± 6.6	24 ± 11	ns	–
	2TCM(2)	19 ± 4.2	9.2 ± 4.5	18 ± 6.7	11 ± 4.2	ns	–
Caudate	2TCM	17 ± 5.4	33 ± 14	19 ± 6.7	51 ± 31	ns	–
	2TCM(2)	18 ± 4.0	10 ± 4.1	18 ± 7.5	23 ± 9.4	ns	–
Midbrain	2TCM	5.7 ± 2.7	40 ± 35	2.8 ± 0.5	23 ± 13	p<0.05	51
	2TCM(2)	2.4 ± 0.3	15 ± 6.9	1.5 ± 0.3	20 ± 11	p<0.001	38

2TCM: the two-tissue compartment model.
2TCM(2): the two-tissue compartment model with K_1/k_2 fixed for cerebellum.
Values are mean ± s.d.
ns: not significant.

caudate, intermediate in the midbrain and low in the cerebellum of the patients with JME (Fig. 3). The binding potential images of a representative control subject and a patient with JME (patient B) are shown in Fig. 1, the images of which were obtained using the automated receptor imaging system (ARIS) with the Logan DVR approach (Odano et al., 2009b). The metabolism of [^{11}C]PE2I was measured in plasma by HPLC. The HPLC chromatogram revealed two radiolabeled metabolites (metabolites I and II). Time-activity curves for fraction (%) of unchanged [^{11}C]PE2I and the two metabolites in plasma are shown in Fig. 4. The metabolism was not rapid but intermediate compared with those of other rapidly metabolized radioligands such as [^{11}C]raclopride, and the fraction of unchanged [^{11}C]PE2I was less than approximately 60% at 10 min after injection in all patients with JME. The trend of these observations was similar to that of normal subjects as shown previously (Jucaite et al., 2006). The individual TAC of unchanged [^{11}C]PE2I fitted by Hill's function was used to establish the metabolite-corrected arterial plasma input, $C_p(t)$.

Tissue-to-plasma concentration ratios, $C_{tissue}(t)/C_p(t)$, (mean ± s.d., n = 8), for each region of the patients with JME are shown in Fig. 5. The ratios for the putamen and caudate tended to increase

Table 5
Comparison of binding potential, BP_{ND}, for [^{11}C]PE2I binding calculated by the simplified reference tissue model and the non-invasive linear graphical approach of the control subjects and patients with JME.

		Control subjects (n = 6)		Patients with JME (n = 8)		Statistics	Mean reduction (%)
Acquisition time		0–63 min		0–58 min			
Reference tissue models		BP_{ND}	(%COV)	BP_{ND}	(%COV)		
Putamen	SRTM	8.0 ± 0.5	5.3 ± 1.3	6.8 ± 1.1	5.4 ± 2.5	p<0.05	15
	Logan DVR	9.4 ± 0.8		7.5 ± 1.2		p<0.01	20
Caudate	SRTM	7.3 ± 1.1	6.5 ± 1.8	6.1 ± 1.1	10.2 ± 2.7	ns	–
	Logan DVR	8.2 ± 1.3		6.9 ± 1.3		ns	–
Midbrain	SRTM	1.6 ± 0.4	11.9 ± 3.2	0.7 ± 0.1	9.1 ± 3.7	p<0.05	56
	Logan DVR	1.6 ± 0.4		0.8 ± 0.1		p<0.05	50

SRTM: simplified reference tissue model.
Logan DVR: non-invasive linear graphic approach.
ns: not significant.
%COVs for Logan DVR were not obtained by this software.

Table 6
Comparison of rate constants and total distribution volume from the two-tissue compartment model with K_1/k_2 fixed for cerebellum for description of [^{11}C]PE2I binding in the control subjects and patients with JME.

Control subjects	0–63 min	K_1	k_2	k_3	k_4	K_1/k_2	V_T
Mean ± s.d. (n = 6)							
Putamen	2TCM(2)	0.35 ± 0.04	0.11 ± 0.02	0.44 ± 0.25	0.02 ± 0.01	3.2 ± 1.0	65 ± 28
Caudate	2TCM(2)	0.30 ± 0.04	0.10 ± 0.02	0.52 ± 0.26	0.03 ± 0.01	3.2 ± 1.0	60 ± 27
Midbrain	2TCM(2)	0.25 ± 0.07	0.07 ± 0.03	0.12 ± 0.03	0.05 ± 0.01	3.2 ± 1.0	11 ± 2.3
Cerebellum	1TCM	0.25 ± 0.05	0.08 ± 0.01			3.2 ± 1.0	
	2TCM	0.30 ± 0.06	0.15 ± 0.03	0.05 ± 0.03	0.06 ± 0.03	2.0 ± 0.4	3.7 ± 0.9
Patients with JME	0–58 min	K_1	k_2	k_3	k_4	K_1/k_2	V_T
Mean ± s.d. (n = 8)							
Putamen	2TCM(2)	0.42 ± 0.09	0.13 ± 0.03	0.34 ± 0.12	0.02 ± 0.01	3.4 ± 0.9	66 ± 31
Caudate	2TCM(2)	0.33 ± 0.05	0.10 ± 0.02	0.28 ± 0.09 *	0.02 ± 0.01 *	3.4 ± 0.9	66 ± 37
Midbrain	2TCM(2)	0.24 ± 0.06	0.07 ± 0.01	0.06 ± 0.02 **	0.04 ± 0.02	3.4 ± 0.9	8.6 ± 1.8
Cerebellum	1TCM	0.30 ± 0.06	0.09 ± 0.02			3.4 ± 0.9	
	2TCM	0.37 ± 0.08	0.21 ± 0.12	0.09 ± 0.10	0.07 ± 0.02	2.1 ± 0.8	4.1 ± 0.9

1TCM: the one-tissue compartment model.
2TCM: the two-tissue compartment model.
2TCM(2): the two-tissue compartment model with K_1/k_2 fixed for cerebellum.
Values are mean ± s.d.
* $p<0.05$.
** $p<0.001$.

during the whole scanning time, however, they reached almost a steady state at 40–60 min for the midbrain and at 20–30 min for the cerebellum. These trends were in agreement with those for normal subjects (Hirvonen et al., 2008).

The time-activity curves for the putamen, the caudate and the midbrain were statistically better described by the 2TCM and the 2TCM(2) than by the 1TCM in all eight patients with JME. The fitted curves for the putamen and the midbrain of a patient with JME and a representative control subject are shown in Figs. 6 and 7 as examples.

For the putamen and the caudate, the three-tissue compartment model (3TCM) did not provide good fitting, thus it was not pursued for further analysis. The rate constants obtained by the 2TCM and the 2TCM(2) for each region of the patients with JME are given in Table 2. The 2TCM(2) provided robust values of binding potential, k_3/k_4, with low %COVs, 5.0–9.0% on average, in each region, showing high reliability. Binding potential for the midbrain of the patients with JME obtained by the 2TCM(2) was 1.4 ± 0.2 (mean ± s.d.).

To compare with binding parameters for control subjects, the PET data of patients with JME acquired for 58 min were calculated. The

Table 7
Comparison of rate constants from the one- and two-tissue compartment models in 58 min data acquisition for description of [^{11}C]PE2I binding in the midbrain of eight patients with JME.

Patient		K_1 (ml/ml/min)	k_2 (min^{-1})	k_3 (min^{-1})	k_4 (min^{-1})	RSS	AIC	SC	F-statistics	
									1TCM/2TCM	1TCM/2TCM(2)
A	1TCM	0.21	0.04			36,668	340	343		
	2TCM	0.26	0.11	0.11	0.06	5109	281	287	$p<0.0001$	
	2TCM(2)	0.25	0.08	0.05	0.05	6653	290	296		$p<0.0001$
B	1TCM	0.20	0.02			73,687	363	366		
	2TCM	0.23	0.06	0.07	0.04	34,882	343	349	$p<0.0001$	
	2TCM(2)	0.23	0.06	0.07	0.04	31,178	339	345		$p<0.0001$
C	1TCM	0.15	0.03			28,621	332	335		
	2TCM	0.19	0.15	0.16	0.05	7465	293	299	$p<0.0001$	
	2TCM(2)	0.17	0.08	0.06	0.04	8796	299	304		$p<0.0001$
D	1TCM	0.19	0.03			73,079	362	365		
	2TCM	0.23	0.10	0.06	0.03	9885	302	308	$p<0.0001$	
	2TCM(2)	0.23	0.08	0.03	0.02	12,836	311	317		$p<0.0001$
E	1TCM	0.23	0.03			65,617	359	362		
	2TCM	0.31	0.13	0.14	0.05	6849	291	296	$p<0.0001$	
	2TCM(2)	0.27	0.06	0.04	0.03	18,473	322	328		$p<0.0001$
F	1TCM	0.29	0.03			153,036	386	389		
	2TCM	0.36	0.12	0.18	0.07	19,723	324	330	$p<0.0001$	
	2TCM(2)	0.32	0.07	0.07	0.06	25,775	333	339		$p<0.0001$
G	1TCM	0.13	0.02			41,950	345	348		
	2TCM	0.16	0.10	0.15	0.04	23,322	330	336	$p<0.0005$	
	2TCM(2)	0.15	0.05	0.08	0.05	28,581	336	342		$p<0.005$
H	1TCM	0.26	0.04			42,566	345	348		
	2TCM	0.36	0.17	0.12	0.04	5172	282	287	$p<0.0001$	
	2TCM(2)	0.32	0.09	0.04	0.03	8693	298	304		$p<0.0001$

1TCM: the one-tissue compartment model.
2TCM: the two-tissue compartment model.
2TCM(2): the two-tissue compartment model with K_1/k_2 fixed for cerebellum.
RSS: residual sum of square.
AIC: Akaike information criterion.
SC: Schwarz criterion.

comparisons of binding potential values are shown in Table 3. Binding potential obtained by the kinetic analyses, k_3/k_4, tended to be larger for 58 min than for 90 min in each region, however, no statistical significance was observed. Binding potentials obtained by the reference tissue models, BP_{ND}, were almost the same and were stable for acquisition time, except for the putamen. The %COVs for 90 min were evidently lower than for 58 min in each region and by each approach. No difference of regional total distribution volume (V_T) was observed, except for the midbrain, in which V_T was slightly lower for 58 min than for 90 min (not shown in the table).

Regional binding parameters for the patients with JME obtained by the kinetic analysis and reference tissue models using data acquired for 58 min were compared with those for the control subjects (Tables 4 and 5). Binding potential was significantly reduced in the midbrain of the patients with JME by all four approaches, the reduction of which was approximately 38–56% on average. For the putamen and caudate, there was no reduction of BP_{ND} values obtained by the kinetic analyses. However, those obtained by the reference tissue models were reduced in the putamen by 15–20% on average. No significant difference of regional total distribution volume was found between patients with JME and normal control subjects. The comparisons of rate constants obtained by the 2TCM(2) for control subjects and the patients with JME are shown in Table 6 because the 2TCM(2) provided more robust and lower %COV values than the 2TCM did. The rate constant k_3 was significantly reduced in the midbrain for the patients with JME. The rate constants in the midbrain of each patient with JME are given in Table 7.

The uptake curves for the cerebellum of all patients with JME, in contrast, were statistically better described by the 3TCM than by the 1TCM and the 2TCM. The fitted curves for 90 min are shown in Fig. 8. The rate constants are given in Tables 2 and 8. In the statistical analyses, the Akaike information criterion and Schwarz criterion score were lower for the 3TCM than for the 2TCM. Moreover, F-statistics rejected the null hypothesis that is that the 2TCM more adequately described radioligand uptake. The rate constants k_3–k_6 were determined with relatively low %COV, 18–35% on average. The values of k_5 and k_6 were larger than those of k_3 and k_4 by one order of magnitude. Since the rate constants k_3 and k_4 are symmetrical to k_5 and k_6 in the three-tissue compartment configuration, it is mathematically difficult to identify which rate constants are for the second or third compartment in cerebellar tissue. The ratios of k_3/k_4 and k_5/k_6 obtained by the 3TCM were 2.1 ± 0.9, and 1.9 ± 1.1 (mean $\pm$ s.d.), respectively, without statistical difference (Table 2). These findings indicated that three kinetically distinguishable compartments exist in the cerebellum.

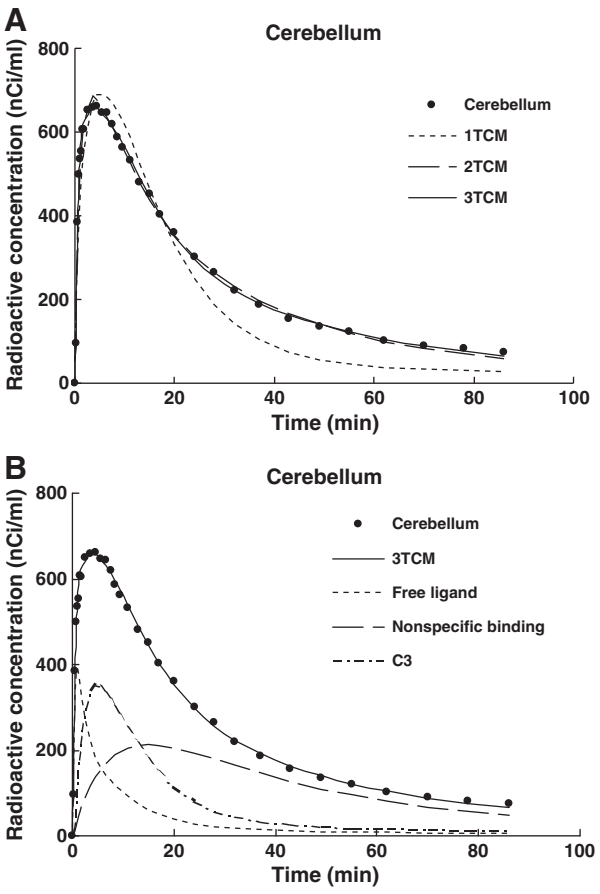

Fig. 8. (A) Radioactivity vs. time in the cerebellum after i.v. injection of [^{11}C]PE2I, and curve fits of the 1TCM, 2TCM and 3TCM (patient B). (B) Total binding, non-specific binding, free radioligand concentration and the third-tissue compartment concentration, C_3 in the cerebellum were estimated by the 3TCM. Note that the third kinetically distinguishable compartment exists in cerebellar tissue and the amount of concentration is not a little.

Discussion

This study shows that binding potential is significantly reduced in the midbrain of patients with JME in comparison with that in age-matched control subjects, all of which were evaluated by kinetic compartment analysis and reference tissue models. The tissue-to-plasma concentration ratio for the midbrain reached an almost steady state at 40–60 min after radioligand injection; hence the binding potential values obtained are reliable. The kinetic analysis validates the use of reference tissue approaches not only in control subjects but also in patients with JME. The findings of reduced DAT binding in the midbrain of the patients with JME indicates impaired dopamine uptake, as discussed in detail in our previous paper (Ciumas et al., 2010).

The present kinetic analysis did not confirm the reduced DAT binding in the putamen; although the mean BP_{ND} values were numerically lower in patients with JME, the difference was not significant. It is noteworthy that the %COV for kinetic analysis was larger and it cannot be ruled out that a large sample is required to confirm reduced density by kinetic analysis, although it is noteworthy that the total volume distribution in the putamen did not differ between the two groups.

The uptake curves of regional [^{11}C]PE2I in the patients with JME are well described by the compartment analyses. For DAT-rich regions such as the putamen, the caudate and the midbrain, the 2TCM gives reliable binding parameter values, and in particular, the 2TCM(2), the two-tissue compartment model with fixed K_1/k_2 ratio derived from the cerebellum, provides robust estimates of values. Hence, the 2TCM with fixed K_1/k_2 is preferable to use for verifying binding parameters obtained by other approaches such as reference tissue models.

Despite the fact that, regarding comparisons of data acquisition for 58 min with that for 90 min in the kinetic analysis, no significant difference was observed in values of binding potential, %COVs of those values for 90 min were evidently lower than for 58 min. and there was no systematic regional difference in this trend. This means that a longer period of data acquisition is preferable to obtain more reliable binding parameters. Indeed, more than 90 min in the acquisition was recommended as an optimal duration (Hirvonen et al., 2008; DeLorenzo et al., 2009). However, the longer the time for data acquisition, the more disadvantageous are increases of noise caused by a short half-life, 20 min for [^{11}C], and by head movement of the subject. Even with the acquisition for 58 min, the 2TCM with fixed K_1/k_2 provided relatively strong and reliable binding parameters in the present study, indicating that the approach is useful to compare values for the patients with JME with those for normal subjects obtained for 63 min.

The reference tissue models also provided robust values for binding potential, when the data for both 58 min and for 90 min were used, except for the putamen. The reason for this exception is unknown, but it may have been caused by the assumption of the reference tissue models, namely, the kinetics of radioligand in the reference region is described by the one-tissue compartment model. However, the kinetics of [^{11}C]PE2I in the reference region, the cerebellum, is described by the two- or three-tissue compartment model. Hence, when the reference tissue models are applied, careful interpretation and validation by other citrine approaches are required.

The three-tissue compartment model was statistically better than the two-tissue compartment model to describe [^{11}C]PE2I binding in the cerebellum (Fig. 8 and Table 8), which means that there are two kinetically distinguishable compartments in cerebellar tissue besides the free radioligand compartment.

The possible explanation for this relates to radioactive metabolites that pass the blood–brain barrier (BBB) of the cerebellum (Farde et al., 1998). [^{11}C]PE2I is metabolized to an intermediate degree after radioligand injection into at least two kinds of radiolabeled metabolites (Fig. 4), which are more polar than unchanged [^{11}C]PE2I (Hirvonen et al., 2008; Jucaite et al., 2006). From study on rodents, these metabolites were identified to be 4-hydroxymethyl analog and 4-carboxyl analog of [^{11}C]PE2I, and the former may penetrate the BBB and potentially bind to DAT (Shetty et al., 2007). Although it is still unknown whether the metabolite passes the BBB in humans as in rodents, the unknown compartment is speculated to correspond to the BBB-passing radiolabeled metabolite in cerebellar tissue.

Another possible explanation of the unknown compartment is structural abnormalities and drug effects as an enzyme-inhibitor in cerebellar tissue of patients with JME. MR volumetry and voxel-based morphometry revealed volume reduction in the thalamus and the cerebellum in the patients with generalized tonic–clonic seizure (Ciumas and Savic, 2006). Diffusion tensor imaging revealed abnormal white matter connectivity in the cerebellum of patients with epileptic seizures (Li et al., 2010). These findings suggest that there is damage to the white matter integrity, which may cause different unknown metabolism of [^{11}C]PE2I in cerebellar tissue of patients with JME.

Since DAT is a presynaptic marker located on the somatodendritic and axon terminal membrane of the DA neurons, and extracellular DA is regulated by the presynaptic D_2 autoreceptors in the substantia nigra (Mortensen and Amara, 2003), the reduced DAT binding in the midbrain may imply impaired DA reuptake. Potential underlying mechanisms include loss of nigral neurons, selective and seizure-related excitotoxic lesions, and the effect of the antiepileptic medication. Neuronal loss in the midbrain seems unlikely because the voxel-based morphometry results did now show any brain atrophy in patients with JME (Ciumas et al., 2008), and because the midbrain, as opposed to the striatum, is not regarded as a primary target for seizure-related excitotoxicity (Deransart and Depaulis, 2002; Gale, 1992).

Valproate, the most commonly used drug among our patients, is reported to increase expression of endogenous DAT gene (Wang et al., 2007), and chronic use of Valproate induces reversible parkinsonism (Armon et al., 1996); however, these findings are incongruent with the results of the present study. Indeed, one of eight patients with JME had no medication, although binding potential was decreased in the midbrain, the same as in other patients. Valproate is also reported to decrease cerebral blood flow (CBF) and cerebral metabolic rate of glucose (Gaillard et al., 1996; Tae et al., 2007). However, no significant difference of the partition coefficient, K_1/k_2 values obtained by the 1TCM in the cerebellum, was observed between control subjects and patients with JME (Table 6), suggesting that CBF alteration did not markedly affect the binding potential values obtained. Thus, our finding may be independent of the antiepileptic medication, and part of the epileptogenic process.

Table 8
Comparison of rate constants from the one-, two- and three-tissue compartment models in 90 min data acquisition for description of [^{11}C]PE2I binding in the cerebellum of eight patients with JME.

Patient		K_1 (ml/ml/min)	k_2 (min^{-1})	k_3 (min^{-1})	k_4 (min^{-1})	k_5 (min^{-1})	k_6 (min^{-1})	RSS	AIC	SC	F-statistics	
											1TCM/2TCM	2TCM/3TCM
A	1TCM	0.26	0.08					37,946	341	344		
	2TCM	0.31	0.15	0.05	0.06			3528	269	275	$p<0.0001$	
	3TCM	0.40	0.71	0.09	0.03	0.93	0.30	1179	238	247		$p<0.0005$
B	1TCM	0.30	0.08					86,927	368	371		
	2TCM	0.39	0.25	0.19	0.10			23,378	330	336	$p<0.0001$	
	3TCM	0.57	0.95	0.11	0.04	0.58	0.15	5238	286	295		$p<0.0001$
C	1TCM	0.25	0.12					46,483	348	351		
	2TCM	0.31	0.21	0.05	0.05			6592	289	295	$p<0.0001$	
	3TCM	0.39	0.82	0.10	0.03	0.91	0.41	3082	269	278		$p<0.0001$
D	1TCM	0.27	0.09					33,439	337	340		
	2TCM	0.31	0.16	0.04	0.04			4770	279	285	$p<0.0001$	
	3TCM	0.37	0.53	0.08	0.03	0.78	0.40	2090	257	265		$p<0.0001$
E	1TCM	0.34	0.07					61,568	357	360		
	2TCM	0.40	0.12	0.03	0.05			2797	262	268	$p<0.0001$	
	3TCM	0.43	0.28	0.06	0.04	0.58	0.50	1608	248	257		$p<0.001$
F	1TCM	0.37	0.08					92,295	370	373		
	2TCM	0.43	0.14	0.05	0.07			5111	281	287	$p<0.0001$	
	3TCM	0.45	0.22	0.05	0.05	0.31	0.46	3349	272	281		$p<0.005$
G	1TCM	0.21	0.07					52,804	352	355		
	2TCM	0.25	0.14	0.05	0.05			4378	276	282	$p<0.0001$	
	3TCM	0.27	0.21	0.02	0.01	0.19	0.18	1718	250	259		$p<0.0001$
H	1TCM	0.38	0.11					21,231	323	326		
	2TCM	0.43	0.16	0.03	0.04			1752	247	253	$p<0.0001$	
	3TCM	0.48	0.36	0.04	0.03	0.46	0.46	1032	234	243		$p<0.0025$

1TCM: the one-tissue compartment model.
2TCM: the two-tissue compartment model.
3TCM: the three-tissue compartment model.
RSS: residual sum of square.
AIC: Akaike information criterion.
SC: Schwarz criterion.

Activation of DA receptors is reported to reduce myoclonic seizures (Greer and Alpern, 1977), and DA dysfunction to induce myoclonias (Vesper et al., 2007); therefore, it seems plausible that both ictal and interictal symptoms in JME involve DA transmission, suggesting a possibility for new treatment strategies, especially with respect to the neurobehavioral problems in patients with JME.

Conclusion

Binding potential for the midbrain of patients with JME was significantly reduced, which was verified by four quantitative approaches. Furthermore, we show that the kinetics of [^{11}C]PE2I in the midbrain does not differ between control subjects and patients with JME other than for specific binding, which further underlines the validity of the conclusion that the DAT binding is impaired in patients with JME. The uptake curves of regional [^{11}C]PE2I in patients with JME could be well described by the compartment analyses. The two-tissue compartment model with fixed K_1/k_2 ratio derived from the cerebellum and reference tissue methods provided robust and reliable estimates of binding parameters. The three-tissue compartment model could best describe uptake in the cerebellum, indicating that two kinetically distinguishable compartments exist in cerebellar tissue, which may correspond to nonspecific binding and the blood–brain barrier-passing metabolite. The kinetic behavior in the cerebellum may be caused by the biochemical nature of the radioligand and potentially by cerebellar structural abnormalities in patients with JME. The reference tissue models are advantageous for clinical studies on the dopamine transporter. Before clinical use, however, the reliability of any simplified methods must be confirmed.

References

Akaike, H., 1974. A new look at the statistical model identification. IEEE Trans. Autom. Control AC-19, 716–723.

Allard, P., Alafuzoff, I., Carlsson, A., Eriksson, K., Ericson, E., Gottfries, C.G., Marcusson, J.O., 1990. Loss of dopamine uptake sites labeled with [^{3}H]GBR-12935 in Alzheimer's disease. Eur. Neurol. 30, 181–185.

Antonini, A., Moresco, R.M., Gobbo, C., De Notaris, R., Panzacchi, A., Barone, P., Calzetti, S., Negrotti, A., Pezzoli, G., Fazio, F., 2001. The status of dopamine nerve terminals in Parkinson's disease and essential tremor: a PET study with the tracer [11-C] FE-CIT. Neurol. Sci. 22, 47–48.

Arakawa, R., Ichimiya, T., Ito, H., Takano, A., Okumura, M., Takahashi, H., Takano, H., Yasuno, F., Kato, M., Okubo, Y., Suhara, T., 2009. Increase in thalamic binding of [(11)C]PE2I in patients with schizophrenia: a positron emission tomography study of dopamine transporter. J. Psychiatr. Res. 43, 1219–1223.

Armon, C., Shin, C., Miller, P., Carwile, S., Brown, E., Edinger, J.D., Paul, R.G., 1996. Reversible parkinsonism and cognitive impairment with chronic valproate use. Neurology 47, 626–635.

Bergstrom, M., Boethius, J., Eriksson, L., Greitz, T., Ribbe, T., Widen, L., 1981. Head fixation device for reproducible position alignment in transmission CT and positron emission tomography. J. Comput. Assist. Tomogr. 5, 136–141.

Carson, R.E., 1986. Parameter estimation in positron emission tomography. In: Phelps, M.E., Mazziota, J.C., Schelbert, H.R. (Eds.), Positron Emission Tomography. Principles and Applications for the Brain and Heart. Raven Press, New York, pp. 347–390.

Chalon, S., Hall, H., Saba, W., Garreau, L., Dollé, F., Halldin, C., Emond, P., Bottlaender, M., Deloye, J.B., Helfenbein, J., Madelmont, J.C., Bodard, S., Mincheva, Z., Besnard, J.C., Guilloteau, D., 2006. Pharmacological characterization of (E)-N-(4-fluorobut-2-enyl)-2beta-carbomethoxy-3beta-(4′-tolyl)nortropane (LBT-999) as a highly promising fluorinated ligand for the dopamine transporter. J. Pharmacol. Exp. Ther. 317, 147–152.

Ciumas, C., Savic, I., 2006. Structural changes in patients with primary generalized tonic and clonic seizures. Neurology 67, 683–686.

Ciumas, C., Wahlin, T.B., Jucaite, A., Lindstrom, P., Halldin, C., Savic, I., 2008. Reduced dopamine transporter binding in patients with juvenile myoclonic epilepsy. Neurology 71, 788–794.

Ciumas, C., Wahlin, T.B., Espino, C., Savic, I., 2010. The dopamine system in idiopathic generalized epilepsies: identification of syndrome-related changes. Neuroimage 51, 606–615.

DeLorenzo, C., Kumar, J.S., Zanderigo, F., Mann, J.J., Parsey, R.V., 2009. Modeling considerations for in vivo quantification of the dopamine transporter using [(11)C]PE2I and positron emission tomography. J. Cereb. Blood Flow Metab. 29, 1332–1345.

Deransart, C., Depaulis, A., 2002. The control of seizures by the basal ganglia? A review of experimental data. Epileptic Disord. 4 (Supple. 3), S61–S72.

Emond, P., Garreau, L., Chalon, S., Boazi, M., Caillet, M., Bricard, J., Frangin, Y., Mauclaire, L., Besnard, J.-C., Guilloteau, D., 1997. Synthesis and ligand binding of nortropane derivatives: N-substituted-2-carbomethoxy-3-(4′-iodophenyl)nortropane and N-(3-iodoprop-2E-enyl)-2-carbomethoxy-3-(3′,4′-disubstitutedphenyl)nortropane. New affinity and selectivity compounds for the dopamine transporter. J. Med. Chem. 40, 1366–1372.

Farde, L., Eriksson, L., Blomquist, G., Halldin, C., 1989. Kinetic analysis of central [^{11}C] raclopride binding to D2-dopamine receptors studied by PET-a comparison to the equilibrium analysis. J. Cereb. Blood Flow Metab. 9, 696–708.

Farde, L., Halldin, C., Müller, L., Suhara, T., Karlsson, P., Hall, H., 1994. PET study of [^{11}C] beta-CIT binding to monoamine transporters in the monkey and human brain. Synapse 16, 93–103.

Farde, L., Ito, H., Swahn, C.G., Pike, V.W., Halldin, C., 1998. Quantitative analyses of carbonyl-carbon-11-WAY-100635 binding to central 5-hydroxytryptamine-1A receptors in man. J. Nucl. Med. 39, 1965–1971.

Gaillard, W.D., Zeffiro, T., Fazilat, S., DeCarli, C., Theodore, W.H., 1996. Effect of valproate on cerebral metabolism and blood flow: an ^{18}F-2-deoxyglucose and ^{15}O water positron emission tomography study. Epilepsia 37, 515–521.

Gale, K., 1992. Subcortical structures and pathways involved in convulsive seizure generation. J. Clin. Neurophysiol. 9, 264–277.

Ginovart, N., Lundin, A., Farde, L., Halldin, C., Backman, L., Swahn, C.G., Pauli, S., Sedvall, G., 1997. PET study of the pre- and post-synaptic dopaminergic markers for the neurodegenerative process in Huntington's disease. Brain 120, 503–514.

Ginovart, N., Meyer, J.H., Boovariwala, A., Hussey, D., Rabiner, E.A., Houle, S., Wilson, A.A., 2006. Positron emission tomography quantification of [^{11}C]-harmine binding to monoamine oxidase-A in the human brain. J. Cereb. Blood Flow Metab. 26, 330–344.

Goodman, M.M., Kilts, C.D., Keil, R., Shi, B., Martarello, L., Xing, D., Votaw, J., Ely, T.D., Lambert, P., Owens, M.J., Camp, V.M., Malveaux, E., Hoffman, J.M., 2000. ^{18}F-labeled FECNT: a selective radioligand for PET imaging of brain dopamine transporters. Nucl. Med. Biol. 27, 1–12.

Greer, C.A., Alpern, H.P., 1977. Mediation of myoclonic seizures by dopamine and clonic seizures by acetylcholine and GABA. Life Sci. 21, 385–392.

Guilloteau, D., Emond, P., Farde, L., 2003. [(11)C]PE2I: a highly selective radioligand for PET examination of the dopamine transporter in monkey and human brain. Eur. J. Nucl. Med. Mol. Imaging 30, 1220–1230.

Gunn, R.N., Sargent, P.A., Bench, C.J., Rabiner, E.A., Osman, S., Pike, V.W., Hume, S.P., Grasby, P.M., Lammertsma, A.A., 1998. Tracer kinetic modeling of the 5-HT1A receptor ligand [carbonyl-^{11}C]WAY-100635 for PET. Neuroimage 8, 426–440.

Halldin, C., Swan, C.-G., Farde, L., Sedvall, G., 1995. Radioligand disposition and metabolism — key information in early drug development. In: Comar, D. (Ed.), PET for Drug Development and Evaluation. Kluwer, Dordrecht, pp. 55–65.

Halldin, C., Farde, L., Lundkvist, C., Ginovart, N., Nakashima, Y., Karlsson, P., Swahn, C.G., 1996. [^{11}C]beta-CIT-FE, a radioligand for quantitation of the dopamine transporter in the living brain using positron emission tomography. Synapse 22, 386–390.

Halldin, C., Erixon-Lindroth, N., Pauli, S., Chou, Y.H., Okubo, Y., Karlsson, P., Lundkvist, C., Olsson, H., Guilloteau, D., Emond, P., Farde, L., 2003. [^{11}C]PE2I — a highly selective radioligand for PET-examination of the dopamine transporter in monkey and human brain. Eur. J. Nucl. Med. Mol. Imaging 30, 1220–1230.

Hill, A.V., 1910. The possible effects of the aggregation of the molecules of haemoglobin on its dissociation curves. J. Physiol. 40, 4–7.

Hirvonen, J., Johansson, J., Teräs, M., Oikonen, V., Lumme, V., Virsu, P., Roivainen, A., Någren, K., Halldin, C., Farde, L., Hietala, J., 2008. Measurement of striatal and extrastriatal dopamine transporter binding with high-resolution PET and [^{11}C]PE2I: quantitative modeling and test–retest reproducibility. J. Cereb. Blood Flow Metab. 28, 1059–1069.

Innis, R.B., Cunningham, V.J., Delforge, J., Fujita, M., Gjedde, A., Gunn, R.N., Holden, J., Houle, S., Huang, S.C., Ichise, M., Iida, H., Ito, H., Kimura, Y., Koeppe, R.A., Knudsen, G.M., Knuuti, J., Lammertsma, A.A., Laruelle, M., Logan, J., Maguire, R.P., Mintun, M.A., Morris, E.D., Parsey, R., Price, J.C., Slifstein, M., Sossi, V., Suhara, T., Votaw, J.R., Wong, D.F., Carson, R.E., 2007. Consensus nomenclature for in vivo imaging of reversibly binding radioligands. J. Cereb. Blood Flow Metab. 27, 1533–1539.

Jucaite, A., Fernell, E., Halldin, C., Forssberg, H., Farde, L., 2005. Reduced midbrain dopamine transporter binding in male adolescents with attention-deficit/hyperactivity disorder: association between striatal dopamine markers and motor hyperactivity. Biol. Psychiatry 57, 229–238.

Jucaite, A., Odano, I., Olsson, H., Pauli, S., Halldin, C., Farde, L., 2006. Quantitative analyses of regional [^{11}C]PE2I binding to the dopamine transporter in the human brain: a PET study. Eur. J. Nucl. Med. Mol. Imaging 33, 657–668.

Laakso, A., Bergman, J., Haaparanta, M., Vilkman, H., Solin, O., Syvalahti, E., Hietala, J., 2001. Decreased striatal dopamine transporter binding in vivo in chronic schizophrenia. Schizophr. Res. 52, 115–120.

Lammertsma, A.A., Hume, S.P., 1996. Simplified reference tissue model for PET receptor studies. Neuroimage 4, 153–158.

Landaw, E.M., DiStefano III, J.J., 1984. Multiexponential, multicompartmental, and noncompartmental modeling. II. Data analysis and statistical considerations. Am. J. Physiol. 246, R665–R677.

Leroy, C., Comtat, C., Trébossen, R., Syrota, A., Martinot, J.L., Ribeiro, M.J., 2007. Assessment of ^{11}C-PE2I binding to the neuronal dopamine transporter in humans with the high-spatial-resolution PET scanner HRRT. J. Nucl. Med. 48, 538–546.

Li, Y., Du, H., Xie, B., Wu, N., Wang, J., Wu, G., Feng, H., Jiang, T., 2010. Cerebellum abnormalities in idiopathic generalized epilepsy with generalized tonic-clonic seizures revealed by diffusion tensor imaging. PLoS One 5 (e152191), 1–7.

Logan, J., Wolf, A.P., Shiue, C.Y., Fowler, J.S., 1987. Kinetic modeling of receptor–ligand binding applied to positron emission tomographic studies with neuroleptic tracers. J. Neurochem. 48, 73–83.

Logan, J., Fowler, J., Volkow, N.D., Wang, G., Ding, Y., Alexoff, D.L., 1996. Distribution volume ratio without blood sampling from graphical analysis of PET data. J. Cereb. Blood Flow Metab. 16, 834–840.

Lundberg, J., Odano, I., Olsson, H., Halldin, C., Farde, L., 2005. Quantification of ^{11}C-MADAM binding to the serotonin transporter in the human brain. J. Nucl. Med. 46, 1505–1515.
Meyer, J.H., Krüger, S., Wilson, A.A., Christensen, B.K., Goulding, V.S., Schaffer, A., Minifie, C., Houle, S., Hussey, D., Kennedy, S.H., 2001. Lower dopamine transporter binding potential in striatum during depression. Neuroreport 12, 4121–4125.
Mintun, M.A., Raichle, M.E., Kilbourn, M.R., Wooten, G.F., Welch, M.J., 1984. A quantitative model for the in vivo assessment of drug binding sites with positron emission tomography. Ann. Neurol. 15, 217–227.
Mortensen, O.V., Amara, S.G., 2003. Dynamic regulation of the dopamine transporter. Eur. J. Pharmacol. 479, 159–170.
Müller, L., Halldin, C., Farde, L., Karlsson, P., Hall, H., Swahn, C.G., Neumeyer, J., Gao, Y., Milius, R., 1993. [^{11}C] beta-CIT, a cocaine analogue. Preparation, autoradiography and preliminary PET investigations. Nucl. Med. Biol. 20, 249–255.
Odano, I., Halldin, C., Karlsson, P., Varrone, A., Airaksinen, A.J., Krasikova, R.N., Farde, L., 2009a. [^{18}F]flumazenil binding to central benzodiazepine receptor studies by PET-quantitative analysis and comparisons with [^{11}C]flumazenil. Neuroimage 45, 891–902.
Odano, I., Sakaguchi, K., Hosoya, Varrone, A., Savic, I., Halldin, C., Farde, L., 2009b. Automated receptor imaging system (AIRIS) in neuroreceptor binding studies with PET. J. Nucl. Med. 50 (Supple.) 174 pp..
Roland, P.E., Graufelds, C.J., Wahlin, J., Ingelman, L., Andersson, M., Ledberg, A., Pedersen, J., Akerman, S., Dabringhaus, A., Zilles, K., 1994. Human brain atlas: for high-resolution functional and anatomical mapping. Hum. Brain Mapp. 1, 173–183.
Schwarz, G., 1978. Estimating the dimension of a model. Ann. Stat. 6, 461–464.
Seki, C., Ito, H., Ichimiya, T., Arakawa, R., Ikoma, Y., Shidahara, M., Maeda, J., Takano, A., Takahashi, H., Kimura, Y., Suzuki, K., Kanno, I., Suhara, T., 2010. Quantitative analysis of dopamine transporters in human brain using [^{11}C]PE2I and positron emission tomography: evaluation of reference tissue models. Ann. Nucl. Med. 24, 249–260.
Shetty, H.U., Zoghbi, S.S., Liow, J.S., Ichise, M., Hong, J., Musachio, J.L., Halldin, C., Seidel, J., Innis, R.B., Pike, V.W., 2007. Identification and regional distribution in rat brain of radiometabolites of the dopamine transporter PET radioligand [^{11}C]PE2I. Eur. J. Nucl. Med. Mol. Imaging 34, 667–678.
Tae, W.S., Joo, E.Y., Han, S.J., Lee, K.H., Hong, S.B., 2007. CBF changes in drug naive juvenile myoclonic epilepsy patients. J. Neurol. 254, 1073–1080.
Varrone, A., Halldin, C., 2010. Molecular imaging of the dopamine transporter. J. Nucl. Med. 51, 1331–1334.
Varrone, A., Steiger, C., Schou, M., Takano, A., Finnema, S.J., Guilloteau, D., Gulyás, B., Halldin, C., 2009. In vitro autoradiography and in vivo evaluation in cynomolgus monkey of [^{18}F]FE-PE2I, a new dopamine transporter PET radioligand. Synapse 63, 871–880.
Vesper, J., Steinhoff, B., Rona, S., Wille, C., Bilic, S., Nikkhah, G., Ostertag, C., 2007. Chronic high-frequency deep brain stimulation of the STN/SNr for progressive myoclonic epilepsy. Epilepsia 48, 1984–1989.
Volkow, N.D., Wang, G.J., Fowler, J.S., Logan, J., Francheschi, D., Maynard, L., Ding, Y.S., Gatley, S.J., Gifford, A., Zhu, W., Swanson, J.M., 2002. Relationship between blockade of dopamine transporters by oral methylphenidate and increase in the extracellular dopamine: therapeutic implications. Synapse 43, 181–187.
Wang, J., Michelhaugh, S.K., Bannon, M.J., 2007. Valproate robustly increases Sp transcription factor-mediated expression of the dopamine transporter gene within dopamine cells. Eur. J. Neurosci. 25, 1982–1986.
Wong, D.F., Gjedde, A., Wagner Jr., H.N., 1986. Quantification of neuroreceptors in the living human brain. I. Irreversible binding of ligands. J. Cereb. Blood Flow Metab. 6, 137–146.
Wong, D.F., Yung, B., Dannals, R.F., Shaya, E.K., Ravert, H.T., Chen, C.A., Chan, B., Folio, T., Scheffel, U., Ricaurte, G.A., 1993. In vivo imaging of baboon and human dopamine transporters by positron emission tomography using [^{11}C]WIN 35,428. Synapse 15, 130–142.
Wong, D.F., Ricaurte, G., Grunder, G., Rothman, R., Naidu, S., Singer, H., Harris, J., Yokoi, F., Villemagne, V., Szymanski, S., Gjedde, A., Kuhar, M., 1998. Dopamine transporter changes in neuropsychiatric disorders. Adv. Pharmacol. 42, 219–223.